Journal of Medicinal Chemistry

pubs.acs.org/jmc

Article

Structure-Guided Chemical Optimization of Bicyclic Peptide (*Bicycle*) Inhibitors of Angiotensin-Converting Enzyme 2

Maximilian A. J. Harman, Steven J. Stanway, Heather Scott, Yuliya Demydchuk, Gustavo Arruda Bezerra, Simone Pellegrino, Liuhong Chen, Paul Brear, Aleksei Lulla, Marko Hyvönen, Paul J. Beswick, and Michael J. Skynner*

Cite This: https://doi.org/10.1021/acs.jmedchem.3c00710

Read Online

ACCESS | Metrics & More | Article Recommendations | Supporting Information

ABSTRACT: Angiotensin-converting enzyme 2 (ACE2) is a metalloprotease that cleaves angiotensin II, a peptide substrate involved in the regulation of hypertension. Here, we identified a series of constrained bicyclic peptides, *Bicycle*, inhibitors of human ACE2 by panning highly diverse bacteriophage display libraries. These were used to generate X-ray crystal structures which were used to inform the design of additional *Bicycles* with increased affinity and inhibition of ACE2 enzymatic activity. This novel structural class of ACE2 inhibitors is among the most potent ACE2 inhibitors yet described *in vitro*, representing a valuable tool to further probe ACE2 function and for potential therapeutic utility.

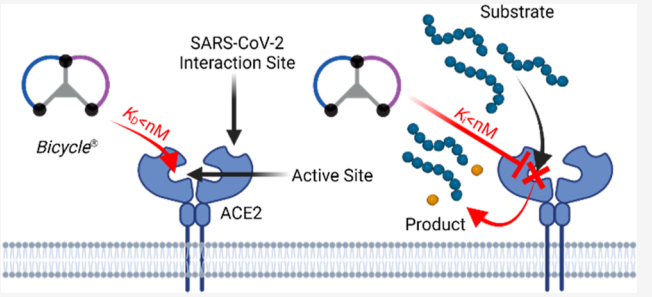

INTRODUCTION

Bicycles are a novel structural class of therapeutics formed by constraining short linear peptides into a stabilized bicyclic structure using a central chemical scaffold.[1] This constraint confers attractive drug-like properties, including high target affinity and specificity, without cross-reactivity even to highly related proteins. *Bicycles* are unlike most small molecules in that they can be readily conjugated, either together or to other payloads, without losing affinity to their designated target. *Bicycles* are also highly amenable to chemical modification, allowing their molecular properties and pharmacology to be tuned using structure−activity relationships (SARs). *Bicycles* are initially identified using a modified bacteriophage display screening platform which is massively diverse, containing $>10^{20}$ unique theoretical exemplars. Here, we looked to use this platform to identify *Bicycles* with inhibitory activity against human angiotensin-converting enzyme 2 (ACE2).

Human ACE2, a major component of the renin−angiotensin−aldosterone system,[2] is a zinc metalloprotease[3] responsible for the cleavage of many natural peptides including bradykinins, neurotensins, and angiotensins.[4] ACE2 has high catalytic activity in cleaving angiotensin II (AngII), a vasopressor and proinflammatory peptide, and lower catalytic activity in angiotensin I (AngI)[5] cleavage. ACE2 is disease associated with ulcerative colitis, where mRNA expression is significantly upregulated, correlated with poor disease outcomes as well as increased inflammation,[6] and as such, inhibition may have a therapeutic utility.

Non-inhibitory, functional ligands to ACE2 have been discovered. XNT[7] was described as an ACE2 activator, and through modeling, it appeared to bind distally to the ACE2 active site, on the outer face of the catalytic domain. Recently, the peptide CPS4[8] was also found to neutralize SARS-CoV-2 infection *in vitro*. Furthermore, potent active-site inhibitors of ACE2 have previously been described.[9−11] DX600 (ACE2 K_i 2.8 nM) is a 26 amino acid cysteine disulfide constrained peptide,[10] and MLN-4760 (ACE2 K_i 0.44 nM) is a small-molecule inhibitor rationally designed from the chemical structure of ACE2's natural substrates.[9] These have been used previously to explore the therapeutic utility of ACE2 inhibition in animal models of human irritable bowel disease (IBD). MLN-4760, at high doses (300 mg/kg, b.i.d) in mice, was disease-modifying in the dextran sodium sulfate (DSS) model[12,13] which points to a potential therapeutic utility for ACE2 inhibitors. However, the high doses used in the study are indicative of suboptimal drug-like properties, and so here we set out to identify improved *Bicycle*-based ACE2 inhibitors.

RESULTS AND DISCUSSION

Identification of Initial *Bicycle* Inhibitors. Phage selections were conducted, as previously described,[1,14] against human ACE2 protein (Figure 1A) and putative ACE2-binding *Bicycles* chemically synthesized and screened (Figure 1B).

Received: April 20, 2023

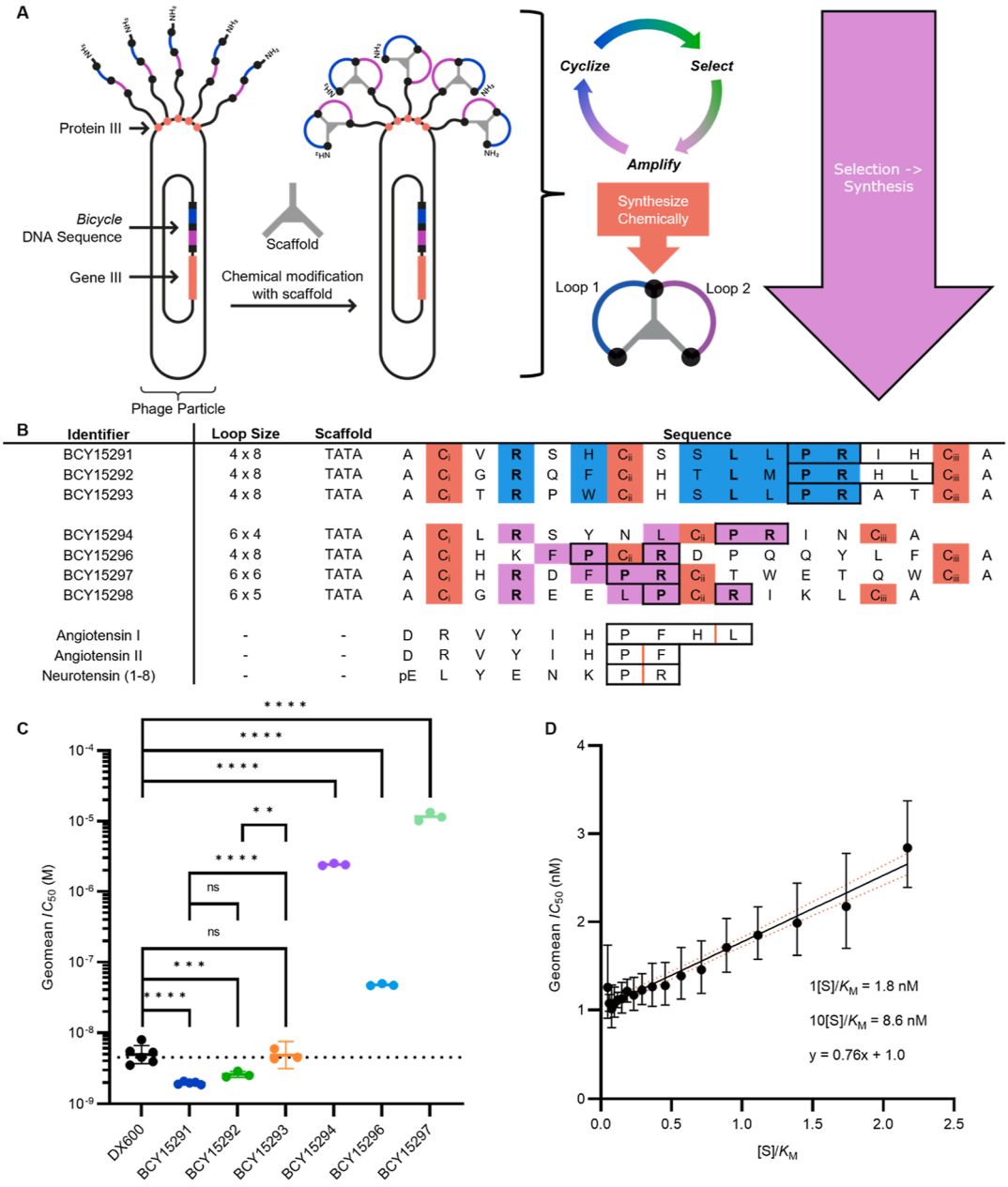

Figure 1. (A) *Bicycle* bacteriophage display process. *Bicycle* encoding sequences were inserted in-frame with gene III to encode linear peptide chains as N-terminal in-frame fusions with coat protein P3 expressed on the surface of the viral particle. Reaction via a symmetrical trivalent chemical scaffold resulted in covalent thioether bond-driven cyclization of the linear peptide chain via the cysteine residues to form a *Bicycle*. The phage, in mixed peptide format libraries, were "panned" against ACE2 via an iterative selection/deselection process based on affinity, and the recovered phage, which specifically bound to ACE2 target material, was subsequently amplified, sequenced, and chemically synthesized. (B) Peptide sequences of recovered phage binding to ACE2 compared to representative substrates of ACE2. Each sequence is denominated by a compound identifier in the form of a BCY number. Three fixed cysteine residues are highlighted in orange and marked in order by subscript by the form "C_x". Blue-shaded sequences had the same loop size and high sequence consensus; purple-shaded sequences shared similar characteristics with different loop sizes and shifted motifs. Bold residues describe the invariant residues observed. All *Bicycle* sequences are displayed from the N- to C-terminus where the N-terminus is a free amine, and the C-terminus is amidated ($CONH_2$—not shown). Loop size was determined by the number of residues between each consecutive cysteine residue excluding the terminal alanine residues. Natural ACE2 substrate sequences are shown at the base of the table for comparison; bordered regions indicate areas of apparent sequence similarity between the substrate and *Bicycle*. Substrate cleavage positions are indicated by vertical red lines. pE refers to pyroglutamyl. (C) IC_{50} determinations of naive *Bicycles* in an ACE2 enzyme inhibition assay using a fluorogenic substrate. Only active sequences are displayed as geometric mean (geomean) IC_{50} ± 95% confidence intervals (CIs), $N \leq 3$. BCY15298 was the only sequence considered inactive and thereby not displayed. The black dotted line marks the geomean IC_{50} of DX600 for comparison. Statistical analysis was performed using a one-way ANOVA; Tukey's multiple-comparison test (ns $p > 0.05$, *$p \leq 0.05$, **$p \leq 0.01$, ***$p \leq 0.001$, and ****$p \leq 0.0001$, with the full statistical summary available in Table S1. A numerical summary of ACE2 of IC_{50} values is available in Table S2. (D) Kinetic assessment of the BCY15291 mechanism of inhibition against the fluorogenic substrate. BCY15291 IC_{50} values were generated ($N = 4$) across 18 substrate concentrations. K_M values generated on each plate were averaged to give a K_M of 37 ± 4.2 μM (mean ± SD) and used to determine values for $[S]/K_M$. Linear regression generated a line with equation $y = 0.76x + 1.0$ used to interpolate IC_{50} values for BCY15291 at $1[S]/K_M$ and $10[S]/K_M$. Orange dotted lines indicate 95% CI of the fitted line.

https://doi.org/10.1021/acs.jmedchem.3c00710
J. Med. Chem. XXXX, XXX, XXX−XXX

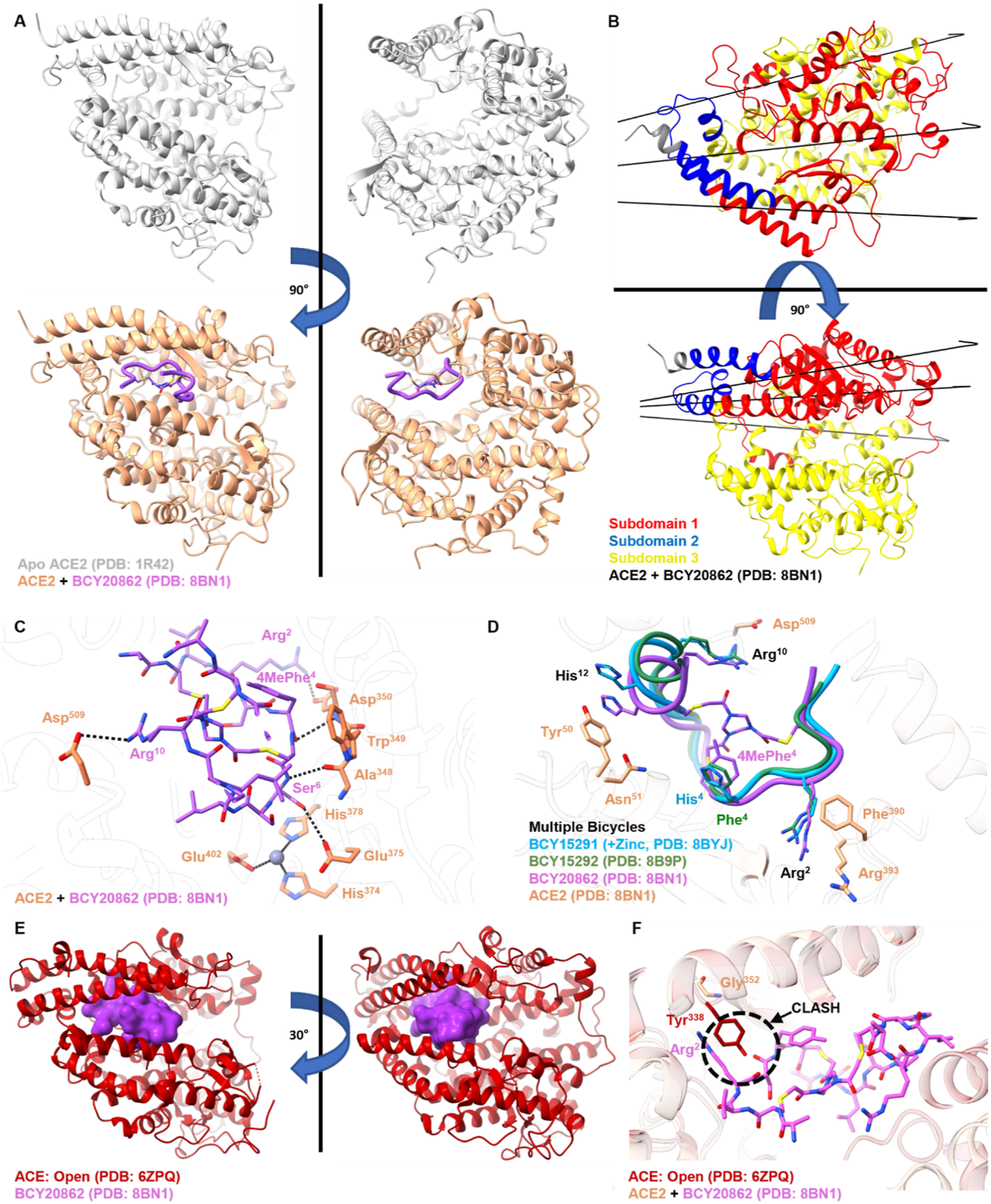

Figure 2. Crystal structures of human ACE2 in complex with *Bicycles* where BCY15291, BCY15292, and BCY20862 are colored blue, green, and purple throughout. (A) Comparison between apo-ACE2 (PDB:1R42) and ACE2:BCY20862 (PDB:8BN1). Two views are represented, 90° laterally rotated from each other, highlighting the pose of the *Bicycle* within the ACE2 binding pocket and the closure of the catalytic cleft. (B) DynDom[18,19] analysis was performed on ACE2:BCY20862 (PDB:8BN1) to superficially deconvolute the receptor−inhibitor dynamics compared to apo-ACE2 (PDB:1R42). DynDom identified three subdomains colored differently for clarity: subdomain 1 (red), subdomain 2 (blue), and subdomain 3 (yellow). (C) Electrostatic interactions established between BCY20862 and ACE2 protein with the zinc catalytic site shown in close proximity. Hydrogen bonds are shown as dashed lines and residues are labeled accordingly to the residue name. (D) Overlay of three crystal structures of this work ACE2:BCY15291 (PDB:8BYJ), ACE2:BCY15292 (PDB:8B9P), and ACE2:BCY20862 (PDB:8BN1), with a view focused on the *Bicycles*. Shared residues between *Bicycles* are colored black and ACE2 residues are colored in wheat. (E) Representation of the BCY20862 (in surface) pose on the apo-ACE open-conformation crystal structure (PDB6ZPQ) (in the cartoon, red). Two views, 30° apart, are presented, indicating BCY20862 size relative to the open ACE catalytic cleft. (F) Selectivity of BCY20862 toward human ACE2 is driven by specific amino acid variation at position 352 (position 338 in ACE). Tyr^{338} (ACE) and Gly^{352} (ACE2) are shown as sticks, while the rest of the protein is in cartoon. BCY20862 in sticks.

https://doi.org/10.1021/acs.jmedchem.3c00710
J. Med. Chem. XXXX, XXX, XXX−XXX

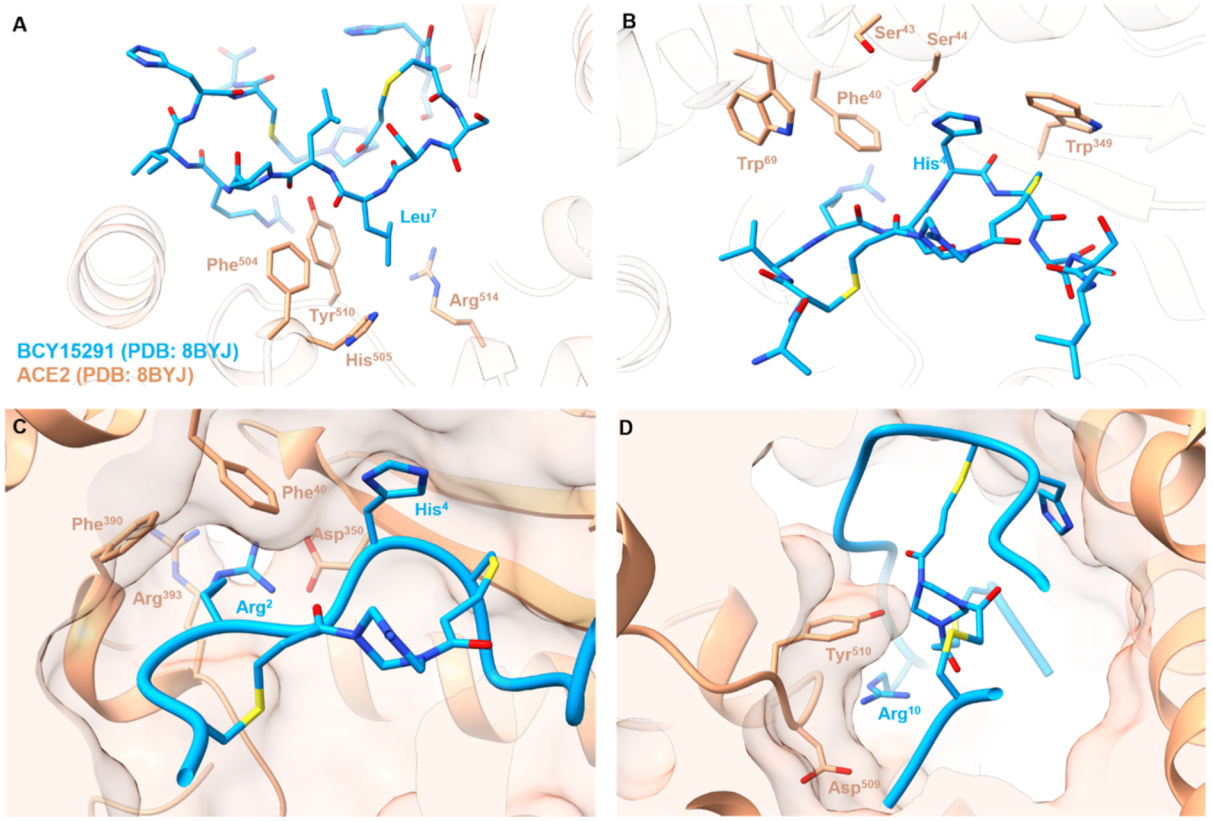

Figure 3. Structure-based rationalization of *Bicycle* optimization. (A) Close-up view of the binding pocket of residue Leu^7 of BCY15291 (blue) on ACE2 (wheat). (B) Close-up view of the binding pocket of residue His^4 of BCY15291 (blue) on ACE2 (wheat). (C) Close-up view of Arg^2 of BCY15291 (blue) engagement within the deep pocket of ACE2 catalytic domain (wheat surface). (D) Close-up view of Arg^{10} of BCY15291 (blue) engagement with delta negative region of the ACE2 catalytic domain (wheat surface). Reference PDB ID: 8BYJ.

BCY15291, BCY15292, and BCY15293 showed a much clearer degree of conservation than the other sequences. This motif enrichment generated the hypothesis that the 4 × 8 loop structure was favorable for binding. There was additional sequence conservation between those *Bicycles* with the motif $C_iXRXXC_{ii}XXLXPRXXC_{iii}$, suggesting that these residues are critical for binding. Minimal conservation was observed between BCY15294, BCY15296, BCY15297, and BCY15298. However, a small motif was shared with the original *Bicycle* sequences, identified as $C_iXR(X)_nPR$. These additional four sequences retained the shared motif across various loop structures. In BCY15296, a heavily shifted motif eradicated what appeared to be a critically conserved arginine residue. The conserved PR is homologous to natural substrates of ACE2, particularly the minor substrate neurotensin (1−8) which undergoes inefficient cleavage at the P|R position. Furthermore, the major substrates of ACE2, angiotensin I and II (AngI and AngII), share homology also, both containing an $R(X)_nPF$ motif. These sequence similarities with the natural substrates suggested that these *Bicycles* may bind within the active site of ACE2.

Bicycles were synthesized and screened for inhibition against $ACE2_{(18-740)}$ under balanced conditions, where substrate concentration was $<2K_M$ (Figure 1C). This confirmed that BCY15291, BCY15292, and BCY15293 potently inhibit ACE2 substrate cleavage with, respectively, significant improvement (BCY15291 $p < 0.0001$; BCY15292 $p = 0.0004$) or comparability (BCY15293 $p > 0.9999$) to DX600. Conversely, BCY15294, BCY15296, and BCY15297 demonstrated significantly reduced inhibition of ACE2 ($p < 0.0001$) compared to DX600 and BCY15293. BCY15298 displayed limited inhibition of ACE2 enzymatic activity with less than 50% inhibition generated with a top concentration of 40,000 nM. BCY15291, BCY15292, and BCY15293 individually generated IC_{50} values of 2.0, 2.6, and 4.9 nM. BCY15291 was not found to be significantly different from BCY15292 ($p = 0.3328$) but was significantly improved over BCY15293 ($p \leq 0.0001$). In comparison to DX600, BCY15293 was identified as not significantly different in inhibitory effects ($p > 0.9999$). BCY15292 was found to be significantly ($p = 0.004$) improved over DX600 in potency; however, BCY15291 was found to be further improved with even greater confidence ($p \leq 0.0001$) than BCY15292. Thereby, BCY15291 was selected for further characterization, SAR analysis, and X-ray crystallography. This data supported the phage sequencing data where sequences with the greatest conservation generated the most active hits.

Investigation of the mechanism of inhibition, using the Mca-APK(Dnp) substrate, showed that BCY15291 appeared to fulfill the criteria of a competitive inhibitor (Figure 1D). A slope of 0.76 nM and y-intercept of 1.0 nM from linear regression were identified and observed as compared to the theoretical K_i of BCY15291, 0.89 nM. Additionally, the IC_{50} for $1[S]/K_M$ was interpolated as 1.8 nM and $10[S]/K_M$ as 8.6 nM, a fold change of 4.8, also indicative of competitive inhibition.[15]

Structural Analyses Support the Mechanism of Action. To elucidate the mechanism of *Bicycle* inhibition and to guide further chemistry optimization, we obtained three $ACE2_{(34-617)}$ cocrystal structures (Table S3) with BCY15291 (PDB:8BYJand8BFW), BCY15292 (PDB:8B9P), and BCY20862 (PDB:8BN1), which is a chemically modified

https://doi.org/10.1021/acs.jmedchem.3c00710
J. Med. Chem. XXXX, XXX, XXX−XXX

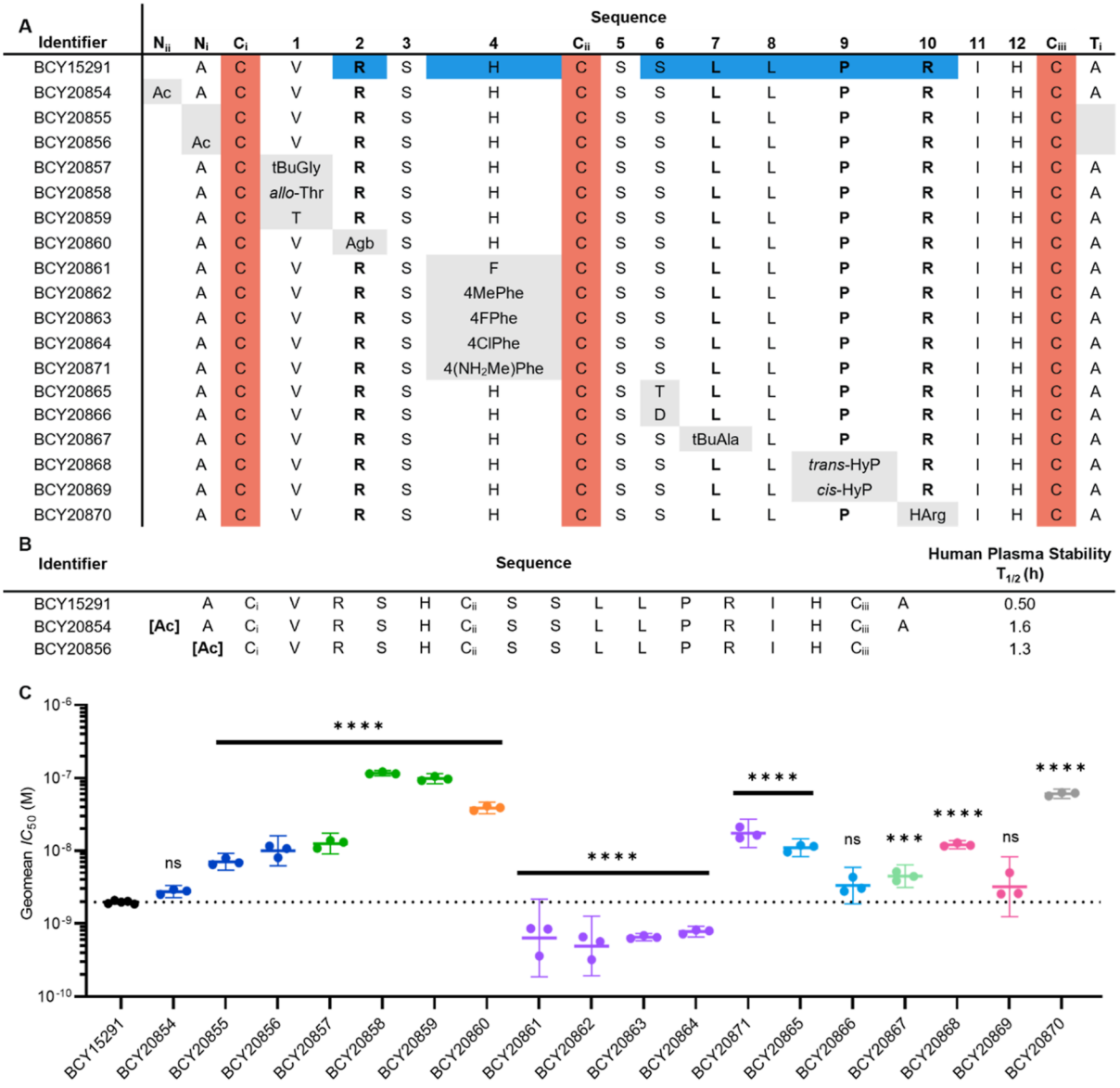

Figure 4. Modification of BCY15291 to improve inhibition potency and plasma stability. (A) Table of chemically modified *Bicycles* designed from the parent sequence BCY15291. Sequences are ordered by the position number of each modification made. Changes from the BCY15291 sequence are highlighted in gray shading. The consensus motif of BCY15291 is shaded in blue, with invariant residues in bold. Three fixed cysteine residues are highlighted in orange. All sequences are displayed from the N- to C-terminus where the N-terminal extensions are described as "N_x", and the C-terminal extensions are described as "T_x." The N- and C-termini are as previously described (free amine or amidated, respectively) unless otherwise specified in the table. Natural amino acids are referred to by their single-letter code. For full names of non-natural amino acids, see the list of abbreviations. (B) *In vitro* human plasma stability ($T_{1/2}$) of key *Bicycle* sequences. Samples analyzed over a 24 h period are expressed as the arithmetic mean of two technical replicates. (C) IC_{50} determinations of chemically modified *Bicycles* in an ACE2 enzyme inhibition assay using a fluorogenic substrate. Each *Bicycle* designed in Figure 4A is displayed as geomean IC_{50} ± 95% CI, $N \geq 3$, and statistically compared to the parental sequence of BCY15291. *Bicycles* are colored depending on the position of the modification made, maintaining the order of the table above. The black dotted line marks the geomean IC_{50} of BCY15291. Statistical analysis was performed using a one-way ANOVA and Tukey's multiple-comparison test (ns $p > 0.05$, *$p \leq 0.05$, **$p \leq 0.01$, ***$p \leq 0.001$, and ****$p \leq 0.0001$). A full statistical summary is available in Table S6. A full summary of IC_{50} values is available in Table S2.

form of BCY15291 (Figure 4A). Each *Bicycle* exhibited well-defined electron density (Figure S1) with the overall structure being similar to that of apo ACE2 (PDB: 1R42[16,17]). There was no significant change in the secondary structure (RMSD of 0.993 Å over 504 superimposed C_α atoms, for the BCY15291:ACE2 complex and apo-ACE2 [PDB:1R42], with the *Bicycles* binding at the active site, located inside the central cleft (Figure 2A). All three *Bicycles* affected the overall structure in a comparable way (RMSD of 0.268 Å over 506 superimposed C_α atoms for BCY15291 and BCY15292 and RMSD of 0.507 Å over 519 superimposed C_α atoms for BCY15291 and BCY20862). As previously described for the inhibitor MLN-4760,[16] the *Bicycles* binding to ACE2 induced a large movement. Ligand-bound ACE2 appeared plastic in this hinge bending, closing uniquely according to the ligand (Tables S4 and S5), with BCY20862 driving alternative conformational change even to its closely related parent BCY15291. Using DynDom[18,19] software, this conformational

https://doi.org/10.1021/acs.jmedchem.3c00710
J. Med. Chem. XXXX, XXX, XXX−XXX

change was described using the rotation movement of three subdomains, with negligible translational contributions (Figure 2B). Interestingly, two of the identified subdomains, 1 and 2, are located in the upper lobe, which contains the conserved catalytic zinc binding site (HEXXH + E motif) observed in the zinc metallopeptidase clan.[20]

Our crystal structures indicate that these *Bicycles* are recognized mainly via polar interactions with residues 347−351, in the vicinity of the catalytic zinc coordination sphere (His^{374}, His^{378}, and Glu^{402}) (Figure 2C). This is the same region ACE2 employs to recognize its natural substrate AngII.[21] Notably, *Bicycle*'s Leu^{7} is accommodated into ACE2 S1 subsite, formed by Phe^{504}, His^{505},Tyr^{510} and Arg^{514}, which has a marked hydrophobic environment (Figure 3A). Seeking to increase potency, we decided to explore the pocket where *Bicycle* His^{4} is bound, which is formed by residues Phe^{40}, Ser^{43}, Ser^{44}, Trp^{69}, and Trp^{349} (Figure 3B). We substituted *Bicycle* His^{4} with the nonproteinogenic amino acid 4-methylphenylalanine (4MePhe), resulting in BCY20862, significantly improving ACE2 affinity. The ACE2:BCY20862 crystal structure indicated minor conformational rearrangements which implicate further inter- and intramolecular stabilization (Figure 2D). The TATA scaffold acquired a twisted boat conformation as opposed to the previously strained chair conformation observed in the BCY15291 structure. While this may come at a minor energy penalty in isolation, we hypothesized that 4MePhe^{4} substitution drives the TATA conformational change, forcing the *Bicycle* C-terminal Ala^{Ti} to adopt a new conformation, which then forces His^{12} to a new position. In BCY15291, His^{12} engages in hydrophobic interactions with ACE2 Tyr^{50}. In the newly adopted conformation in BCY20862, *Bicycle* His^{12} engages in hydrophobic interactions with *Bicycle* Leu^{8} and *Bicycle* Pro^{9} as well as ACE2 Val^{343}. These new intermolecular interactions and a further set of intramolecular contacts from 4MePhe^{4} and TATA likely surmount the original energy penalty and possibly would drive increases in *Bicycle* affinity. Overlays of *Bicycle* pairs (Figure S2A−C) highlight that the introduction of Phe-like residues can drive scaffold reorientation. Next, we compared ACE2 and the canonical ACE in complex with *Bicycles* to predict selectivity. The most striking feature is ACE's central cleft, in which the open conformation is narrower than that of ACE2 in the open conformation.[22] Superposition of BCY20862 onto open conformation ACE clearly shows that due to the narrower cleft, the active site access by the *Bicycle* is very unfavorable (Figure 2E). If ACE can have a more open conformation in solution than that reported in its crystal structure,[22] the *Bicycles* could access the active site, but substitution of Gly^{352} in ACE2 by Tyr^{338} in ACE would still result in steric clashes with *Bicycle* Arg^{2}, preventing binding to ACE (Figure 2F).

Optimization of *Bicycle In Vitro* Human Plasma Stability. Positive initial hits from phage led us to consider an optimal target product profile. A suite of first-generation structure-guided sequence modifications were synthesized (Figure 4A) to explore both plasma stability (Figure 4B) and improved potency (Figure 4C). We observed poor stability for BCY15291, with a $T_{1/2}$ of 0.5 h in human plasma, which required optimization. The first rationalization was to evaluate removal of the N- and C-terminal Ala residues with and without addition of an N-terminal acetyl (Ac) group. These exogenous amino acids, residual from the bacteriophage selection process, may be proteolytically unstable[23] in the blood and, thereby, contribute to poor *in vitro* and *in vivo* plasma stability. Generally, acetylation of either the Cys^{Ci} or Ala N-terminus can be protective toward degradation, assuming that these modifications are favorable for target engagement. Removal of both the N- and C-terminal Ala residues (des Ala, BCY20855) as well as N-terminal acetylation of the des Ala peptide (BCY20866) was found to be not favorable ($p \leq 0.0001$) with IC_{50} values of 7.0 and 10 nM. However, the N-terminal acetylation of the original hit peptide (BCY20854) had no significant effect on ACE2 inhibition with an IC_{50} of 2.7 nM ($p = 0.6491$). N-terminal acetylation, with or without terminal alanine residues (BCY20854 or BCY20856), resulted in slightly improved stability, demonstrating a $T_{1/2}$ of 1.6 and 1.3 h, respectively. This supports the notion that exocyclic alanine residues of bicyclic peptides may be subject to proteolytic degradation. A $T_{1/2}$ of 1.6 h was found to be suitable for early progression given that *Bicycles* are mostly subject to rapid renal clearance.

Sequence- and Structure-Guided Potency Optimization. A distinguishing feature between BCY15291, BCY15292, and BCY15293 is that they all contain differing aromatic residues at His^{4}, Phe^{4}, and Trp^{4}, respectively. Therefore, a range of substituted phenylalanine residues were introduced at this position including 4-chlorophenylalanine (4ClPhe), 4-fluorophenylalanine (4FPhe), 4-methylphenylalanine (4MePhe), and 4-aminomethylphenylalanine (4(NH_2Me)-Phe). The latter was hoped to form intramolecular interaction with the TATA scaffold, potentially through hydrophobic contacts with the scaffold ring core. The 4(NH_2Me)Phe group could also potentially form a hydrogen bonding interaction with either the C-terminal amide ($CONH_2$) or the Cys^{Ciii} amide. This His^{4} residue in BCY15291 only partially fills the space fringed by the C-terminal Ala^{Ti} and Met^{62}. Incorporation of these larger groups could also afford a favorable interaction with these said residues. 4MePhe substitution (BCY20862) was more potent ($p < 0.0001$) with an IC_{50} of 0.49 nM. The BCY20862 cocrystal structure revealed that the backbone of the peptide and the central scaffold had moved slightly to accommodate this residue, including Ala^{Ti} which previously looked to make stabilizing intramolecular hydrophobic interactions. This showed potential to make the des Ala modification in combination with the 4MePhe^{4} substitution, given that no other N- or C-terminal Ala interactions were observed, at no loss of activity, unlike the case of BCY20856. Phe^{4} (BCY20861), 4ClPhe^{4} (BCY20863), and 4FlPhe^{4} (BCY20864) replacements were also all found to have significantly improved enzyme inhibition ($p \leq 0.0001$) over BCY15291, with IC_{50} values of 0.64, 0.65, and 0.78 nM, respectively. No significant difference ($p \geq 0.3312$ in all cases) was observed between these four substitutions. The 4-(NH_2Me)Phe^{4} substituent (BCY20871) was not as well tolerated, showing a loss in potency ($p \leq 0.0001$) with an IC_{50} to 17 nM, suggesting that the gains in replacing His^{4} with the larger phenylalanine are offset by a potentially poor interaction of the aniline group with residues in this region. Overall, Phe-like substitutions in this position are well tolerated with minor para ring position extensions. However, such extensions providing hydrophilicity or shifts in electronegativity contributed little to the overall improvement.

BCY15291's cocrystal structure revealed position Val^{1}, poorly conserved across BCY15291, BCY15292, and BCY15293, and was oriented slightly away from two small hydrophobic pockets. Substitution by *tert*-butylglycine

https://doi.org/10.1021/acs.jmedchem.3c00710
J. Med. Chem. XXXX, XXX, XXX−XXX

Table 1. Summary of Key Affinity Constants for All *Bicycles*[a]

		ACE2			ACE	
Identifier	Sequence	K_i (nM)	IC_{50} (nM)	K_D (nM)	IC_{50} (μM)	K_D (μM)
BCY15291	ACVRSHCSSLLPRIHCA	0.89	2.0	0.44	>40	>10
BCY15292	ACGRQFCHTLMPRHLCA	1.2	2.6	1.2	22	3.8
BCY15293	ACTRPWCHSLLPRATCA	2.2	4.9	1.6	>40	>10
BCY15294	ACLRSYNLCPRINCA	1100	2400	850	>40	>10
BCY15296	ACHKFPCRDPQQYLFCA	21	47	29	>40	5.1
BCY15297	ACHRDFPRCTWETQWCA	5200	12,000	11,000	33	0.35
BCY15298	ACGREELPCRIKLCA	-	>40,000	>10,000	>40	>10
BCY20854	[**Ac**]ACVRSHCSSLLPR1HCA	1.2	2.7	0.72	>40	>10
BCY20855	CVRSHCSSLLPRIHC	3.2	7.0	1.7	>40	9.5
BCY20856	[**Ac**]CVRSHCSSLLPRIHC	4.5	10	2.7	>40	>10
BCY20857	AC[**tBuGly**]RSHCSSLLPRIHCA	5.7	13	2.5	>40	>10
BCY20858	AC[**AlloThr**]RSHCSSLLPRIHCA	53	120	36	>40	>10
BCY20859	AC**T**RSHCSSLLPRIHCA	44	98	25	>40	>10
BCy20860	ACV[**Agb**]ASHCSSLLPRIHCA	18	39	9.1	>40	>10
BCY20861	ACVRS**F**CSSLLPRIHCA	0.29	0.64	0.060	>40	>10
BCY20862	ACVRS[**4MePhe**]CSSLLPRIHCA	0.22	0.49	0.049	>40	>10
BCY20863	ACVRS[**4FPhe**]CSSLLPRIHCA	0.30	0.65	0.057	>40	>10
BCY20864	ACVRSP[**4ClPhe**]CSSLLPRIHCA	0.35	0.78	0.054	>40	>10
BCY20871	ACVRSP[**NH_2Phe**]CSSLLPRIHCA	7.9	17	11	>40	>10
BCY20865	ACVRSHCS**T**LLPRIHCA	5.0	11	8.3	>40	>10
BCY20866	ACVRSHCS**D**LLPRIHCA	1.5	3.3	1.9	>40	>10
BCY20867	ACVRSHCSS[**tBuAla**]LPRIHCA	2.0	4.5	3.1	>40	>10
BCY20868	ACVRSHCSSLL[**HyP**]IRIHCA	5.5	12	11	>40	>10
BCY20869	ACVRSHCSSLL[**Cis-HyP**]RIHCA	1.5	3.2	1.3	>40	>10
BCY20870	ACVRSHCSSLLP[**HArg**]1HCA	27	61	52	>40	>10

[a]*Bicycle* data are presented as two groups: first primary naive hits, and second, chemically modified iterations of BCY15291. Theoretical inhibition constants (K_i) for ACE2 are presented as Cheng−Prusoff corrected geomean IC_{50} via the Cheng−Prusoff equation $K_i = IC_{50}/(1 + ([S]/K_M))$ using geomean K_M = 33 μM and [S] = 40 μM assuming a competitive inhibition modality. Geomean IC_{50} and K_D values for ACE2 and ACE are also presented. Further details for these values may be found in Tables S2 and S8 for ACE2 and Tables S7 and S9 for ACE, respectively.

(tBuGly) could potentially provide a better orientation for engagement with these pockets by the addition of a third methyl group to the valine side chain. Alternatively, Thr and its *allo*-Thr derivative could be potentially incorporated to introduce greater polarity and even hydrogen bonding to a resident crystal water molecule. Interestingly, although all substitutions resulted in significant ($p < 0.0001$) loss in activity, the Thr[1] and *allo*-Thr[1] substitutions were significantly less well tolerated at 98 and 120 nM IC_{50}, respectively (both $p < 0.0001$) in comparison to the tBuGly[1] analogue at 13 nM, suggesting that hydrophilicity is not tolerated at this position.

Arg[2] was found to be fully engaged with the ACE2 protein (Figure 3C), interacting with several residues in a small pocket including Phe[40], Phe[390], and Arg[393] (itself forming a salt bridge interaction with Glu[37]). A salt bridge interaction is also observed with Asp[350]. The crystal structure of BCY15291 revealed a strain in the Cys^{Ci}-TATA scaffold amide bond. We postulated that the introduction of the smaller 2-amino-4-guanidinobutyric acid (Agb) may potentially relieve this amide bond strain and allow the *Bicycle* backbone to adopt a more favorable conformation while maintaining these key interactions with the ACE2 protein. The Agb[2] analogue (BCY20860) was found to have a significant loss in potency at an IC_{50} value of 39 nM ($p < 0.0001$), suggesting that this change results in a decreased interaction with the key residues in this pocket.

The Ser[6]'s hydroxyl group is oriented away from a series of well-defined waters in the BCY15291 structure. The hydroxyl group occupies a small pocket created by the Cys^{Cii} side chain and Leu[8]. Replacement of this residue with a Thr could potentially orient the hydroxyl group toward the crystal waters and allow the Thr methyl group to reside in this small hydrophobic pocket. Alternatively, introduction of an Asp residue could orientate the side chain acid away from the small hydrophobic pocket toward the waters in the active site. This would introduce a similar hydrophilic interaction while controlling the strong net positive charge of the *Bicycle*. Interestingly, Asp[6] was tolerated with no significant change in IC_{50}, 3.3 nM ($p = 0.0531$), whereas Thr[6] was significantly less so at 11 nM ($p < 0.0001$). This highlighted a potential negative sensitivity to hydrophobic residues at this position, while hydrophilicity and charge were tolerated.

Leu[7] sits in a small pocket ringed by ACE2's Phe[504], His[505], and Arg[514], along with face-to-face interaction with Tyr[510]. Although facing into the reasonably hydrophilic pocket, Leu[7] was close to filling this space. *tert*-Butylalanine (tBuAla) could potentially expand deeper into this pocket and further improve binding affinity. The inhibition data for the tBuAla[7] modification (BCY20867) in this case revealed a modest loss in potency, shifting to IC_{50} 4.5 nM ($p < 0.001$), which highlighted that further hydrophobicity may not drive a greater gain in activity despite reasonable spatial tolerance.

At the entrance to the active site, Pro[9] faces the bulk solvent. This presented an opportunity to introduce hydrophilicity at this position, such as a hydroxyl group which may aid solubility and reduce the hydrophobic effect. It was anticipated that a *cis*- or *trans*-hydroxyproline (*cis*-HyP or *trans*-HyP) may face their hydroxyl group toward a nearby water molecule to introduce

https://doi.org/10.1021/acs.jmedchem.3c00710
J. Med. Chem. XXXX, XXX, XXX−XXX

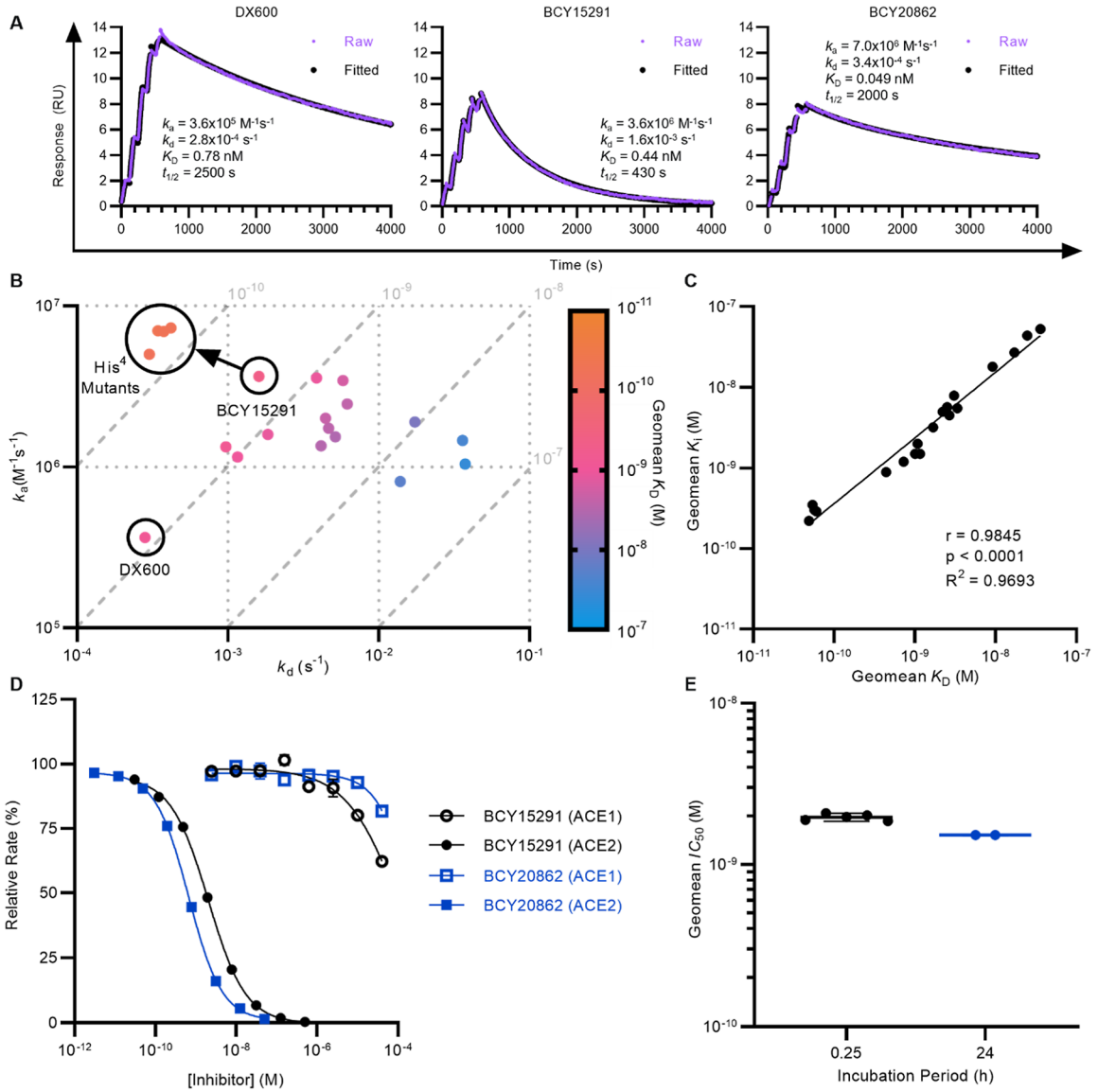

Figure 5. (A) Comparison of BCY15291, BCY20862, and DX600 binding kinetics to ACE2, as determined by surface plasmon resonance studies using the peptides as analytes to the immobilized ACE2 ligand. Sensorgram traces (purple lines) presented with injection and flow fill ranges removed, fitted with the 1:1 binding model (black lines). Kinetic constants k_a, k_d, and K_D are presented as geomean average values. Half-life ($t_{1/2}$) values were calculated ($t_{1/2} = \ln(2)/k_d$). All data $N \geq 3$. The full dataset is available in Table S8. All χ^2 values were determined as <1% of observed R_{max}, indicating a close fit. (B) Affinity plot comparing association and dissociation profiles of *Bicycles* and DX600 as determined by SPR assays. Gray diagonal lines and associated numbering indicate K_D (in M) boundaries whereby the geomean K_D of each *Bicycle* is represented by the color gradient. Orange represents increased ACE2 affinity, and blue represents reduced ACE2 affinity between the range of 10^{-11} and 10^{-7} M. Favorable changes in binding kinetics are highlighted between parental BCY15291 and His^4 substitutions (excluding BCY20871). (C) A Pearson correlation test compares independently generated K_i (Cheng−Prusoff corrected geomean IC_{50}) and K_D values, fit by simple linear regression, for BCY15291 and all analogues. (D) Comparison of ACE and ACE2 inhibition with representative *Bicycles* to demonstrate selectivity using fluorogenic substrates. Normalized ACE2 (filled symbols) and ACE (open symbols) enzyme inhibition data is representative of duplicates (mean ± SD). The top concentration tested against ACE was 40 μM *Bicycle*. All data $N \geq 2$. (E) Enzyme inhibition study, using a fluorogenic substrate, to investigate the propensity for BCY15291 to be metabolized by ACE2 as a substrate. BCY15291 was incubated with ACE2 protein for up to 24 h following which IC_{50} values across different incubation periods were determined. Data is displayed as geomean IC_{50} ± 95% CI, $N \geq 2$.

these improved properties. The *cis*-HyP^9 conformer was tolerated here with no significant change in activity, IC_{50} 3.2 nM ($p > 0.0964$), as opposed to the *trans*-HyP^9 counterpart which caused a reduction in affinity with IC_{50} 12 nM ($p < 0.0001$).

Arg^{10} adopts an electrostatic interaction with Asp^{509} (Figure 3D), along with a hydrogen bonding network with several crystal water molecules. In addition, there appears to be an interaction with one of the TATA amide bonds. Arginine residues potentially have proteolytic stability issues, and it was felt that replacement of this residue could be advantageous. A homoarginine (HArg) was introduced at this position with a view to maintaining the electrostatic interaction with Asp^{509} and the extended hydrogen bonding network with water. This HArg^{10} substitution (BCY20870) was found to have significantly reduced binding affinity with an IC_{50} 61 nM ($p < 0.0001$), suggesting that these favorable interactions were disrupted.

https://doi.org/10.1021/acs.jmedchem.3c00710
J. Med. Chem. XXXX, XXX, XXX−XXX

The phage platform, utilizing impressive loop residue randomization, serves to generate its own structure−activity relationship insights through well-defined motif consensus. Highlighting position 4, we observed that the sequence variability between BCY15291, BCY15292, and BCY15293 behaved as a powerful indicator for medicinal chemistry affinity optimization. Alternatively, the core conserved RXXC$_{ii}$XXLXPR residues appeared to be extremely well optimized for target affinity with no substitutions driving improvement in potency. Nonproteinogenic substitutions where successfully tolerated can provide highly beneficial physical−chemical properties, driving improved stability, reducing plasma protein binding, and even increasing solubility when introducing appropriate charge or greater polarity. For these *Bicycles*, the emphasis on medicinal chemistry can be hereon focused on the physical−chemical improvements, as opposed to driving affinity, given their innate potency.

Deeper Investigation of Advanced Compounds. Affinity and binding kinetics for ACE2 and ACE were determined for all *Bicycles* where possible (Table 1), with exemplar sensorgrams of DX600, BCY15291, and BCY20862 highlighted (Figure 5A). DX600 demonstrated a high affinity for ACE2 with a K_D of 0.78 nM and a long binding half-life ($t_{1/2}$) of 2500 s. Comparatively to DX600, BCY15291 was of higher affinity with a K_D of 0.44 nM, driven by an increase of an order of magnitude in the association rate (k_a) of 3.6×10^6 M^{-1} s^{-1} compared to DX600 (k_a of 3.6×10^5 M^{-1} s^{-1}). BCY15291 also exhibited a relatively fast dissociation rate (k_d) of 1.6×10^{-3} s^{-1} causing it to have a shorter $t_{1/2}$ of 430 s. The 4MePhe substitution in BCY20862 appeared to not only help improve the association rate constant, 7.0×10^6 M^{-1} s^{-1}, to ACE2 but also extended residency time through an improved k_d of 3.4×10^{-4} s^{-1}, resulting in a $t_{1/2}$ of 2000 s and an overall affinity of K_D 0.049 nM.

Affinity plot analysis revealed that, except for BCY20870, all Phe-like substitutions at His^4 of BCY15291 resulted in minor increases in the association rate and even greater changes in the dissociation rate (Figure 5B). Across all changes in affinity, the *Bicycles* retained very fast association kinetics and the overall affinity change was driven by the dissociation kinetics. DX600 comparatively appeared most reliant on slow dissociation kinetics for target affinity. *Bicycles* in this case confer a potential advantage over macrocycles like DX600 for cardiovascular targets, whereby fast association kinetics to initiate a direct pharmacodynamic response are ideal but with added optionality of tunable dissociation kinetics, allowing for a tailored receptor residency time. A positive linear correlation ($r = 0.98$, $p < 0.0001$) was observed between the values for geomean K_D and the geomean K_i, for BCY15291 and its derivatives (Figure 5C). The strong correlation here further supports the competitive mechanism of action.

Selectivity of these key *Bicycles* for ACE2 over ACE was assessed using enzyme inhibition studies. BCY15291 and BCY20862 did not reach IC_{50} for ACE cleavage of Mca-RPPGFSAFK(Dnp) at concentrations up to 40000 nM, the highest tested (Figure 5D). This indicated that BCY15291 showed >20,000-fold selectivity for ACE2, and BCY20862 showed >81,000-fold selectivity for ACE2 inhibition, as expected from our structural rationalizations.

Given the homology of BCY15291's sequence to natural substrate cleavage sites, the stability of ACE2 inhibition by BCY15291 was also investigated (Figure 5E). The IC_{50} after 24 h of incubation at 25 °C with the enzyme was 1.5 nM as compared to the 0.25 h incubations with IC_{50} 2.0 nM. This gives confidence that there is no cleavage of the *Bicycle* by ACE2 and is supported by the crystal structures where the orientation of the sequence is such that the PR region is shifted away from ACE2's catalytic center.

CONCLUDING REMARKS

Here, picomolar-affinity competitive antagonists of ACE2 enzyme function were developed and optimized. These *Bicycles* appeared to drive significant conformational change within ACE2, resulting in the formation of a stabilized ternary complex, amenable to study via high-resolution X-ray crystallography. The work described provides an overview of how phage selection hits can be rapidly optimized to produce compounds with attractive drug-like properties, namely, high potency and good physical chemistry, and builds on our experience optimizing compounds to other targets.[14,24,25] The cocrystal structures highlighted multiple inter- and intramolecular contributions from the *Bicycles*. These were used to lead chemical optimization, negating the need to resort to traditional Ala or DAla scans. The structure-guided design allowed rationalization of significant 10-fold affinity improvements through simple, singular, nonproteinogenic amino acid substitutions, demonstrating the modularity of the peptide structure. The 4-methylphenylalanine substitution allowed further stabilization, demonstrating how the *Bicycle* can perpetuate intramolecular interaction to enhance its binding stability, delivering rapid association and extended dissociation rates from the target. The net output from this work is a set of improved compounds for the further study of ACE2 function and its potential role in disease,[26] most notably IBD.

EXPERIMENTAL SECTION

Bacteriophage Selections. Bacteriophage selections utilized Avitag biotinylated human ACE2 (ACROBiosystems, AC2-H82E6) as the target material. 27 phage libraries displaying peptides cyclized with a TATA scaffold were exposed to the target material. Various loop sizes were used to house randomized natural amino acid residues between selectively conserved cysteines. Target-bound phage particles were enriched, separated, and sequenced using previously described methods to identify sequences of interest.[1,14]

Solid-Phase Peptide Synthesis. Peptides were synthesized as previously described.[27] Analytical traces are available within the Supporting Information. Compounds were isolated at a >80% purity by HPLC.

Production of ACE2 for Crystallography. The DNA encoding for the catalytic domain of human ACE2 (UniProt[28] Q9BYF1, amino acid residues 19−615) was cloned into the pExp-xMBP-TEV-CHis vector to yield the expression construct of ACE2 with the N-terminal fusion to maltose-binding protein (MBP) followed by TEV protease cleavage site and possessing C-terminal 8xHis tag (pExp-xMBP-TEV-ACE2-CHis plasmid was deposited to Addgene as entry #194998). The ACE2 expression plasmid was transformed into SHuffle T7 Express cells (NEB). The large-scale protein expression was started in 2xYT media supplemented with 100 μg/mL ampicillin at 37 °C. After the cultures reached OD600 of 0.6−1, the medium was supplemented with 0.3 mM $ZnCl_2$ and 0.4 mM IPTG and the protein expression was allowed to proceed for 14−16 h at 18 °C. The cells were harvested, resuspended in lysis buffer containing 50 mM sodium phosphate pH 8.0, 500 mM NaCl, and 20 mM imidazole, supplemented with 250 μg/mL DNaseI and 1 mM PMSF, and lysed using an Avestin EmulsiFlex C-5 homogenizer. The lysate cleared by centrifugation at 40,000*g* was loaded onto a gravity flow column with 5 mL of PureCube Ni-NTA agarose resin (Cube Biotech) equilibrated in a wash buffer (50 mM sodium phosphate pH 8.0, 300 mM NaCl, and 20 mM imidazole). The resin was washed first with 10 column

https://doi.org/10.1021/acs.jmedchem.3c00710
J. Med. Chem. XXXX, XXX, XXX−XXX

volumes (CV) of high-salt buffer containing 50 mM sodium phosphate pH 8.0, 1000 mM NaCl, and 20 mM imidazole and then with 10 CV of wash buffer, and the protein was eluted in 5 CV of a wash buffer supplemented with 250 mM imidazole. The Ni-eluate was loaded onto a gravity flow column with 5 mL of amylose resin (NEB); the resin was washed with 10 CV of wash buffer (as before), and the protein was eluted in the same buffer with the addition of 20 mM maltose. The MBP fusion partner was cleaved off by TEV protease (produced in-house). To remove MBP, the protein solution after TEV protease cleavage was reapplied to the Ni-NTA resin, and after washing, the ACE2-CHis protein was eluted in a buffer containing 50 mM sodium phosphate pH 8.0, 300 mM NaCl, and 250 mM imidazole. The eluted protein was concentrated to 1 mL using Amicon Ultra-15 concentrator with a cutoff of 50 kDa and loaded onto size-exclusion HiLoad Superdex 200 16/600 pg column (Cytiva) equilibrated in 20 mM Tris−HCl pH 7.2, 200 mM NaCl. The peak fractions containing ACE2-CHis were pooled, and the protein was concentrated to 10 mg/mL using the 50 kDa cutoff Amicon Ultra-15 concentrator and used for crystallization trials.

ACE2 Crystallization, Data Collection, and Structure Determination. Cocrystals of ACE2 and *Bicycles* were generated by screening ACE2 at 14.5/mL in 20 mM Tris-acetate pH 7.2, 200 mM NaCl, and 1 mM *Bicycles* using the LMB, BCS, Wizard I&II, and JCSG + screens (Molecular Dimensions). Drops were set up using the mosquito robotics system (SPT Labtech) with 0.2 μL of the protein solution and 0.2 μL of the screen solution using the sitting-drop vapor-diffusion method. Crystals were observed in several conditions, which are summarized hereafter: for ACE2 + BCY15291 (in the presence of zinc), crystals were obtained in 0.2 M ammonium citrate dibasic and 20% w/v poly(ethylene glycol) 3350; for ACE2 + BCY15291 (in the absence of zinc), crystals were obtained in 0.1 M sodium acetate pH 4.6, 0.02 M calcium chloride dihydrate, and 30% v/v 2-methyl-2,4-pentanediol; for ACE2 + BCY20862, crystals were obtained in 0.1 M Tris pH 8.0, 0.2 M magnesium chloride hexahydrate, 10% v/v glycerol, and 25% v/v poly(ethylene glycol) smeared high; the ACE2 + BCY15292 crystals were obtained in 0.1 M sodium acetate pH 4.6, 0.02 M calcium chloride dihydrate and 30% v/v 2-methyl-2,4-pentanediol. For crystallization of ACE2 + BCY15291 in the presence of zinc, 10 mM (final concentration) $ZnCl_2$ was added prior to crystallization. The crystals were cryo-cooled in liquid nitrogen in the same solution for data collection. X-ray diffraction data was collected at Diamond synchrotron radiation sources (beamline IO4) and then processed using the pipedream package by Global Phasing Ltd; structures were solved using Phaser[29] from the CCP4 package.[30] Models were iteratively refined and rebuilt by using Refmac[31] and Coot[32] programs. Ligand coordinates and restraints were generated from their SMILES strings using the AceDRG[33] software from the CCP4 package.[30] Figures 2, 3, and S2 panels were generated using UCSF ChimeraX version 1.4.[34] Figure S1 was generated using PyMOL version 2.5.2. Figure 2B and Tables S4 and S5 were generated using DynDom v1.5.[18,19]

ACE and ACE2 Enzyme Inhibition. Inhibition studies were performed in 50 mM HEPES, 150 mM NaCl, 1 μM $ZnCl_2$, 0.015% Triton X-100, and 2.5% DMSO in black-walled 384-well assay plates. Human $ACE2_{(18-740)}$ protein (ACROBiosystems, AC2-H52H8, >95% purity) at 5.0 pM was incubated with a duplicate titration of *Bicycle* from a maximum concentration of 40 μM for a period of 15 min. Subsequently, 40 μM (final assay concentration) of the Mca-APK(Dnp) substrate (Merck Life Science UK Ltd, SML2948) was added to initiate the enzymatic reaction. The ACE2 concentration was such that ≤15% product was formed and that product formation was linear with respect to time for the assay duration. Upon cleavage of the substrate at the Pro−Lys peptide linkage, the fluorescence of Mca was observed via fluorescence intensity at an excitation wavelength of 320 nm and an emission wavelength of 400 nm using a PHERAstar FS/FSX (BMG Labtech) plate reader. The initial rates of substrate cleavage were determined for each *Bicycle* titration point over a 75 min time course with 91 s cycle intervals. These were normalized to low (substrate only) and high (ACE2 with substrate) references and fit via nonlinear regression analysis using the following model: "log(inhibitor) vs response − variable slope (four parameters)" in GraphPad Prism v9.5.0 (730) to determine an IC_{50}. Human somatic $ACE_{(30-1261)}$ protein (Bio-Techne Ltd, 929-ZN-010, >95% purity) at 60 pM was assayed similarly using an Mca-RPPGFSAFK-(Dnp) substrate (Merck Life Science UK Ltd, SCP0131) at 2.5 μM (final assay concentration). The ACE concentration was such that ≤15% product was formed and that product formation was linear with respect to time for the assay duration. A 12 min time course was used. DX600 was supplied by Cambridge Bioscience (CAY22186).

ACE2 Enzyme Inhibition Stability. The same protocol was used as per the above with the following adjustments. The titration of *Bicycle* was incubated with the ACE2 protein dilution in a clear 96-well plate at a total volume of 150 μL and sealed using an aluminum plate seal to minimize the effects of evaporation. This plate was incubated at 25 °C for 24 h before samples were used in the inhibition assay described previously.

***Bicycle* Mechanism of Inhibition of ACE2.** Mechanistic studies were conducted using the same conditions described for the enzyme inhibition studies. Replicate 18-point titrations of the Mca-APK(Dnp) substrate (80−1.8 μM) were cross-titrated against replicate titrations (200−0.064 nM) of the *Bicycle* inhibitor. ACE2 protein was also incubated with the same substrate titration in the absence of an inhibitor with further controls including substrate titration alone, ACE2 and *Bicycle* titration alone, ACE2 alone, and buffer alone. Data for each substrate concentration and inhibitor titration was fit via nonlinear regression analysis using the following model: "log(inhibitor) vs response − variable slope (four parameters)." IC_{50} values generated were plotted against $[S]/K_M$ and fit by simple linear regression. All analyses were performed in GraphPad Prism v9.5.0 (730).

Surface Plasmon Resonance. SPR analysis was performed on a Biacore T200 (Cytiva). In brief, human ACE2 protein was immobilized on a Series S Sensor Chip CM5 (Cytiva, 29104988) using standard primary amine-coupling chemistry at 25 °C with HBS-P+ (10 mM HEPES, 0.15 M NaCl, 0.05% v/v surfactant P20), 1 μM $ZnCl_2$, 1% DMSO, pH 7.4 as the running buffer. The carboxymethyl dextran surface was activated with a 7 min injection of a 1:1 v/v ratio of 0.4 M 1-ethyl-3-(3-dimethylaminopropyl) carbodiimide hydrochloride (EDC)/0.1 M *N*-hydroxy succinimide (NHS) at a flow rate of 10 μL min^{-1}. ACE2 protein was diluted to 40 nM in 10 mM sodium acetate (pH 4.5) and captured with 150 s contact time at 5 μL min^{-1}. Residual activated groups were blocked with a 7 min injection of 1 M ethanolamine pH 8.5. Surface densities of 800−1000 RU were achieved. To determine the affinity for ACE2, a 5-point titration of *Bicycle* underwent single-cycle kinetic evaluation at 25 °C, a flow rate of 30 or 40 μL/min, with an association time of 60 s and a dissociation time of up to 7200 s. Data were solvent-corrected for DMSO bulk effects. A 50% DMSO wash was included between cycles to minimize sample carryover. All data were double-reference-corrected against the reference flow cell and matched buffer blanks. Data processing and kinetic fitting were performed using Biacore T200 Evaluation Software v3.1. Data were fitted using the 1:1 binding model or steady-state affinity model where appropriate. GraphPad Prism v9.5.0 (730) was used to display the data. Human ACE protein was diluted to a concentration of 100 nM before capture as described above. *Bicycles* were assayed again as above except for using a multiple-cycle kinetic format with an 8-point titration.

***In Vitro* Human Plasma Stability.** Pooled frozen plasma was thawed in a water bath at 37 °C prior to performing the experiment. The plasma was centrifuged at 4000 rpm for 5 min, and any clots were removed. Finally, the pH was adjusted to 7.4 ± 0.1. The test compounds were made up to 100 μM in DMSO. The positive control, propantheline, was prepared at 100 μM by diluting a 5 μL DMSO stock solution with 45 μL of ultrapure water and 450 μL of 45% MeOH/H_2O. 98 μL of blank plasma was spiked with 2 μL of dosing solution (100 μM) to achieve a 2 μM final concentration in duplicate, and samples were incubated at 37 °C in a water bath. At each time point (0, 1, 2, 4, 6, and 24 h), 100 μL of 4% H_3PO_4 and then 800 μL of the stop solution (200 ng/mL tolbutamide and 200 ng/mL labetalol in 100% MeOH) were added to precipitate the protein and

https://doi.org/10.1021/acs.jmedchem.3c00710
J. Med. Chem. XXXX, XXX, XXX−XXX

then mixed thoroughly. The samples were then centrifuged at 4000 rpm for 10 min and an aliquot of supernatant (100 μL) was transferred for LC−MS/MS analysis. The % remaining of the test compound after incubation in plasma was calculated using the following equation: % remaining = 100 × (peak area ratio at appointed incubation time/peak area ratio at T_0 time). The half-life ($T_{1/2}$) was calculated from the log linear plot of the concentration versus time.

Statistical Analyses. GraphPad Prism v9.5.0 (730) was used to analyze ACE2 enzyme inhibition data. Ordinary one-way ANOVA and Tukey−Kramer multiple-comparison tests were used to evaluate for a significant mean difference between $\log_{10}$-transformed IC_{50} values. A family-wise alpha threshold and a confidence level of α = 0.001 (99.9% confidence interval) were used. Multiplicity-adjusted P values were reported. In all cases, the ANOVA summary F-test found a significant difference ($p < 0.0001$) between means. The Brown−Forsythe test also indicated no significant difference ($p \geq 0.05$) between standard deviations.

■ ASSOCIATED CONTENT

Supporting Information

The Supporting Information is available free of charge at https://pubs.acs.org/doi/10.1021/acs.jmedchem.3c00710.

Structural data, biochemical and biophysical constants, confidence intervals, statistical analyses, and HPLC traces (PDF)

Molecular formula strings (SMILES) (CSV)

■ AUTHOR INFORMATION

Corresponding Author

Michael J. Skynner − *BicycleTx Ltd., Cambridge CB21 6GS, U.K.*; Email: michael.skynner@bicycletx.com

Authors

Maximilian A. J. Harman − *BicycleTx Ltd., Cambridge CB21 6GS, U.K.*; orcid.org/0000-0002-3667-5929

Steven J. Stanway − *BicycleTx Ltd., Cambridge CB21 6GS, U.K.*

Heather Scott − *BicycleTx Ltd., Cambridge CB21 6GS, U.K.*; orcid.org/0000-0001-6936-9330

Yuliya Demydchuk − *BicycleTx Ltd., Cambridge CB21 6GS, U.K.*

Gustavo Arruda Bezerra − *BicycleTx Ltd., Cambridge CB21 6GS, U.K.*; orcid.org/0000-0003-4471-821X

Simone Pellegrino − *BicycleTx Ltd., Cambridge CB21 6GS, U.K.*; orcid.org/0000-0001-6302-2774

Liuhong Chen − *BicycleTx Ltd., Cambridge CB21 6GS, U.K.*

Paul Brear − *Department of Biochemistry, University of Cambridge, Cambridge CB2 1GA, U.K.*; orcid.org/0000-0002-4045-0474

Aleksei Lulla − *Department of Biochemistry, University of Cambridge, Cambridge CB2 1GA, U.K.*

Marko Hyvönen − *Department of Biochemistry, University of Cambridge, Cambridge CB2 1GA, U.K.*; orcid.org/0000-0001-8683-4070

Paul J. Beswick − *BicycleTx Ltd., Cambridge CB21 6GS, U.K.*

Complete contact information is available at: https://pubs.acs.org/10.1021/acs.jmedchem.3c00710

Author Contributions

Atomic coordinates for the four crystal structures obtained have been deposited to the RCSB Protein Data Bank with the following accession codes: 8BYJ [ACE2 + BCY15291 (in the presence of zinc)]; 8BFW [ACE2 + BCY15291 (in the absence of zinc)]; 8BN1 (ACE2 + BCY20862); 8B9P (ACE2 + BCY15292). The authors will release the atomic coordinates upon article publication. All authors contributed to and approved the final version of the manuscript. M.J.S., P.J.B., and M.A.J.H., conceptualization. Y.D., bacteriophage selections. M.A.J.H., biochemical and biophysical assays. A.L., P.B., and M.H., protein crystallography. G.A.B. and S.P., structural analysis. S.J.S., medicinal chemistry. M.A.J.H., writing the original draft. M.J.S., P.J.B., M.H., L.C., M.A.J.H., S.J.S., and H.S., manuscript review and editing.

Funding

Innovate UK—73786.

Notes

The authors declare the following competing financial interest(s): MAJH, SJS, HS, YD, GAB, SP, LC, PJB and MJS were full time employees of Bicycle Therapeutics at the time that the work was conducted and may therefore own stock or be eligible for stock options in Bicycle Therapeutics. MAJH, SJS, YD, LC, PJB and MJS are named inventors on patent application(s) relating to compounds described in this work.

■ ACKNOWLEDGMENTS

The authors would like to acknowledge the following persons: the *Bicycle* Therapeutics chemistry team and WuXi AppTec for synthesis of the compounds studied, Professor Jody Mason and Dr. Peter Brown for helpful conversations, Dr. Rachel Dods also for structural analyses, and lastly, Alistair Milnes for laboratory assistance. They are grateful for access to the X-ray crystallographic facility at the Department of Biochemistry and for the Diamond Light Source for access to beamline I04 (proposal mx25402). Graphical abstract was created with BioRender.com.

■ ABBREVIATIONS

4MePhe, 4-methyl-phenylalanine
4FPhe, 4-fluoro-phenylalanine
4ClPhe, 4-chlorophenylalanine
4(NH_2Me)Phe, 4-(aminomethyl)phenylalanine
Ac, acetyl
ACE, angiotensin-converting enzyme
ACE2, angiotensin-converting enzyme 2
Agb, 2-amino-4-guanidinobutyric acid
AngI, angiotensin I
AngII, angiotensin II
ANOVA, analysis of variance
CI, confidence interval
cis-HyP, *cis*-L-4-hydroxyproline
CV, column volume
Dnp, 2,4-dinitrophenyl
DSS, dextran sodium sulfate
EDC, 1-ethyl-3-(3-dimethylaminopropyl) carbodiimide hydrochloride
Geomean, geometric mean
HArg, homoarginine
HEPES, 2-[4-(2-hydroxyethyl)piperazin-1-yl]ethanesulfonic acid
IBD, irritable bowel disease
k_a, association rate constant
k_d, dissociation rate constant
K_D, equilibrium dissociation constant
LCI, lower confidence interval
MBP, maltose-binding protein

https://doi.org/10.1021/acs.jmedchem.3c00710
J. Med. Chem. XXXX, XXX, XXX−XXX

Mca, 7-methoxycoumarin-4-acetyl
NaCl, sodium chloride
NHS, *N*-hydroxy-succinimide
R_{max}, maximum response
RU, response units
SAR, structure−activity relationship
TATA, triacryloylhexahydro-*s*-triazine
tBuAla, *tert*-butyl-alanine
tBuGly, *tert*-butyl-glycine
trans-HyP, *trans*-L-4-hydroxyproline
UCI, upper confidence interval
$ZnCl_2$, zinc chloride

REFERENCES

(1) Heinis, C.; Rutherford, T.; Freund, S.; Winter, G. Phage-Encoded Combinatorial Chemical Libraries Based on Bicyclic Peptides. *Nat. Chem. Biol.* **2009**, *5*, 502−507.
(2) Oudit, G. Y.; Crackower, M. A.; Backx, P. H.; Penninger, J. M. The Role of ACE2 in Cardiovascular Physiology. *Trends Cardiovasc. Med.* **2003**, *13*, 93−101.
(3) Donoghue, M.; Hsieh, F.; Baronas, E.; Godbout, K.; Gosselin, M.; Stagliano, N.; Donovan, M.; Woolf, B.; Robison, K.; Jeyaseelan, R.; Breitbart, R. E.; Acton, S. A Novel Angiotensin-Converting Enzyme-Related Carboxypeptidase (ACE2) Converts Angiotensin I to Angiotensin 1-9. *Circ. Res.* **2000**, *87*, e1−e9.
(4) Danilczyk, U.; Penninger, J. M. Angiotensin-Converting Enzyme II in the Heart and the Kidney. *Circ. Res.* **2006**, *98*, 463−471.
(5) Guy, J. L.; Jackson, R. M.; Acharya, K. R.; Sturrock, E. D.; Hooper, N. M.; Turner, A. J. Angiotensin-Converting Enzyme-2 (ACE2): Comparative Modeling of the Active Site, Specificity Requirements, and Chloride Dependence. *Biochemistry* **2003**, *42*, 13185−13192.
(6) Potdar, A. A.; Dube, S.; Naito, T.; Li, K.; Botwin, G.; Haritunians, T.; Li, D.; Casero, D.; Yang, S.; Bilsborough, J.; Perrigoue, J. G.; Denson, L. A.; Daly, M.; Targan, S. R.; Fleshner, P.; Braun, J.; Kugathasan, S.; Stappenbeck, T. S.; McGovern, D. P. B. Altered Intestinal ACE2 Levels Are Associated With Inflammation, Severe Disease, and Response to Anti-Cytokine Therapy in Inflammatory Bowel Disease. *Gastroenterology* **2021**, *160*, 809−822.e7.
(7) Hernández Prada, J. A.; Ferreira, A. J.; Katovich, M. J.; Shenoy, V.; Qi, Y.; Santos, R. A. S.; Castellano, R. K.; Lampkins, A. J.; Gubala, V.; Ostrov, D. A.; Raizada, M. K. Structure-Based Identification of Small-Molecule Angiotensin-Converting Enzyme 2 Activators as Novel Antihypertensive Agents. *Hypertension* **2008**, *51*, 1312−1317.
(8) Adhikary, P.; Kandel, S.; Mamani, U.-F.; Mustafa, B.; Hao, S.; Qiu, J.; Fetse, J.; Liu, Y.; Ibrahim, N. M.; Li, Y.; Lin, C.-Y.; Omoscharka, E.; Cheng, K. Discovery of Small Anti-ACE2 Peptides to Inhibit SARS-CoV-2 Infectivity. *Adv. Ther.* **2021**, *4*, 2100087.
(9) Dales, N. A.; Gould, A. E.; Brown, J. A.; Calderwood, E. F.; Guan, B.; Minor, C. A.; Gavin, J. M.; Hales, P.; Kaushik, V. K.; Stewart, M.; Tummino, P. J.; Vickers, C. S.; Ocain, T. D.; Patane, M. A. Substrate-Based Design of the First Class of Angiotensin-Converting Enzyme-Related Carboxypeptidase (ACE2) Inhibitors. *J. Am. Chem. Soc.* **2002**, *124*, 11852−11853.
(10) Huang, L.; Sexton, D. J.; Skogerson, K.; Devlin, M.; Smith, R.; Sanyal, I.; Parry, T.; Kent, R.; Enright, J.; Wu, Q. L.; Conley, G.; DeOliveira, D.; Morganelli, L.; Ducar, M.; Wescott, C. R.; Ladner, R. C. Novel Peptide Inhibitors of Angiotensin-Converting Enzyme 2. *J. Biol. Chem.* **2003**, *278*, 15532−15540.
(11) Mores, A.; Matziari, M.; Beau, F.; Cuniasse, P.; Yiotakis, A.; Dive, V. Development of Potent and Selective Phosphinic Peptide Inhibitors of Angiotensin-Converting Enzyme 2. *J. Med. Chem.* **2008**, *51*, 2216−2226.
(12) Guzman, L.-M.; Boiselle, C. A.; Odate, S.; Gross, S. B.; Picarella, D.; Byrnes, J.; Ellard, C.; Bourque, L. K.; Donahue, S. S1669 Gl1001 Attenuation of Acute Colitis in a Mouse DSS Model Is Associated with Inhibition of Its Target, ACE2. *Gastroenterology* **2009**, *136*, A-246.
(13) Byrnes, J. J.; Gross, S.; Ellard, C.; Connolly, K.; Donahue, S.; Picarella, D. Effects of the ACE2 Inhibitor GL1001 on Acute Dextran Sodium Sulfate-Induced Colitis in Mice. *Inflammation Res.* **2009**, *58*, 819−827.
(14) Baeriswyl, V.; Rapley, H.; Pollaro, L.; Stace, C.; Teufel, D.; Walker, E.; Chen, S.; Winter, G.; Tite, J.; Heinis, C. Bicyclic Peptides with Optimized Ring Size Inhibit Human Plasma Kallikrein and Its Orthologues While Sparing Paralogous Proteases. *ChemMedChem* **2012**, *7*, 1173−1176.
(15) Buker, S. M.; Boriack-Sjodin, P. A.; Copeland, R. A. Enzyme−Inhibitor Interactions and a Simple, Rapid Method for Determining Inhibition Modality. *SLAS Discovery* **2019**, *24*, 515−522.
(16) Towler, P.; Staker, B.; Prasad, S. G.; Menon, S.; Tang, J.; Parsons, T.; Ryan, D.; Fisher, M.; Williams, D.; Dales, N. A.; Patane, M. A.; Pantoliano, M. W. ACE2 X-Ray Structures Reveal a Large Hinge-Bending Motion Important for Inhibitor Binding and Catalysis. *J. Biol. Chem.* **2004**, *279*, 17996−18007.
(17) Berman, H. M.; Westbrook, J.; Feng, Z.; Gilliland, G.; Bhat, T. N.; Weissig, H.; Shindyalov, I. N.; Bourne, P. E. The Protein Data Bank. *Nucleic Acids Res.* **2000**, *28*, 235−242.
(18) Hayward, S.; Berendsen, H. J. Systematic Analysis of Domain Motions in Proteins from Conformational Change: New Results on Citrate Synthase and T4 Lysozyme. *Proteins* **1998**, *30*, 144−154.
(19) Hayward, S.; Kitao, A.; Berendsen, H. J. Model-Free Methods of Analyzing Domain Motions in Proteins from Simulation: A Comparison of Normal Mode Analysis and Molecular Dynamics Simulation of Lysozyme. *Proteins* **1997**, *27*, 425−437.
(20) Rawlings, N. D.; Barrett, A. J. Evolutionary Families of Metallopeptidases. *Methods Enzymol.* **1995**, *248*, 183−228.
(21) Masuyer, G.; Schwager, S. L. U.; Sturrock, E. D.; Isaac, R. E.; Acharya, K. R. Molecular Recognition and Regulation of Human Angiotensin-I Converting Enzyme (ACE) Activity by Natural Inhibitory Peptides. *Sci. Rep.* **2012**, *2*, 717.
(22) Cozier, G. E.; Lubbe, L.; Sturrock, E. D.; Acharya, K. R. Angiotensin-converting Enzyme Open for Business: Structural Insights into the Subdomain Dynamics. *FEBS J.* **2021**, *288*, 2238−2256.
(23) Gonda, D. K.; Bachmair, A.; Wünning, I.; Tobias, J. W.; Lane, W. S.; Varshavsky, A. Universality and Structure of the N-End Rule. *J. Biol. Chem.* **1989**, *264*, 16700−16712.
(24) Teufel, D. P.; Bennett, G.; Harrison, H.; van Rietschoten, K.; Pavan, S.; Stace, C.; le Floch, F.; van Bergen, T.; Vermassen, E.; Barbeaux, P.; Hu, T. T.; Feyen, J. H. M.; Vanhove, M. Stable and Long-Lasting, Novel Bicyclic Peptide Plasma Kallikrein Inhibitors for the Treatment of Diabetic Macular Edema. *J. Med. Chem.* **2018**, *61*, 2823−2836.
(25) Rhodes, C. A.; Pei, D. Bicyclic Peptides as Next-Generation Therapeutics. *Chem.—Eur J.* **2017**, *23*, 12690−12703.
(26) Eder, M.; Pavan, S.; Bauder-Wüst, U.; van Rietschoten, K.; Baranski, A.-C.; Harrison, H.; Campbell, S.; Stace, C. L.; Walker, E. H.; Chen, L.; Bennett, G.; Mudd, G.; Schierbaum, U.; Leotta, K.; Haberkorn, U.; Kopka, K.; Teufel, D. P. Bicyclic Peptides as a New Modality for Imaging and Targeting of Proteins Overexpressed by Tumors. *Cancer Res.* **2019**, *79*, 841−852.
(27) Mudd, G. E.; Brown, A.; Chen, L.; van Rietschoten, K.; Watcham, S.; Teufel, D. P.; Pavan, S.; Lani, R.; Huxley, P.; Bennett, G. S. Identification and Optimization of EphA2-Selective Bicycles for the Delivery of Cytotoxic Payloads. *J. Med. Chem.* **2020**, *63*, 4107−4116.
(28) Bateman, A.; Martin, M.-J.; Orchard, S.; Magrane, M.; Ahmad, S.; Alpi, E.; Bowler-Barnett, E. H.; Britto, R.; Bye-A-Jee, H.; Cukura, A.; Denny, P.; Dogan, T.; Ebenezer, T.; Fan, J.; Garmiri, P.; da Costa Gonzales, L. J.; Hatton-Ellis, E.; Hussein, A.; Ignatchenko, A.; Insana, G.; Ishtiaq, R.; Joshi, V.; Jyothi, D.; Kandasaamy, S.; Lock, A.; Luciani, A.; Lugaric, M.; Luo, J.; Lussi, Y.; MacDougall, A.; Madeira, F.; Mahmoudy, M.; Mishra, A.; Moulang, K.; Nightingale, A.; Pundir, S.; Qi, G.; Raj, S.; Raposo, P.; Rice, D. L.; Saidi, R.; Santos, R.; Speretta, E.; Stephenson, J.; Totoo, P.; Turner, E.; Tyagi, N.; Vasudev, P.;

https://doi.org/10.1021/acs.jmedchem.3c00710
J. Med. Chem. XXXX, XXX, XXX−XXX

Warner, K.; Watkins, X.; Zaru, R.; Zellner, H.; Bridge, A. J.; Aimo, L.; Argoud-Puy, G.; Auchincloss, A. H.; Axelsen, K. B.; Bansal, P.; Baratin, D.; Batista Neto, T. M.; Blatter, M.-C.; Bolleman, J. T.; Boutet, E.; Breuza, L.; Gil, B. C.; Casals-Casas, C.; Echioukh, K. C.; Coudert, E.; Cuche, B.; de Castro, E.; Estreicher, A.; Famiglietti, M. L.; Feuermann, M.; Gasteiger, E.; Gaudet, P.; Gehant, S.; Gerritsen, V.; Gos, A.; Gruaz, N.; Hulo, C.; Hyka-Nouspikel, N.; Jungo, F.; Kerhornou, A.; le Mercier, P.; Lieberherr, D.; Masson, P.; Morgat, A.; Muthukrishnan, V.; Paesano, S.; Pedruzzi, I.; Pilbout, S.; Pourcel, L.; Poux, S.; Pozzato, M.; Pruess, M.; Redaschi, N.; Rivoire, C.; Sigrist, C. J. A.; Sonesson, K.; Sundaram, S.; Wu, C. H.; Arighi, C. N.; Arminski, L.; Chen, C.; Chen, Y.; Huang, H.; Laiho, K.; McGarvey, P.; Natale, D. A.; Ross, K.; Vinayaka, C. R.; Wang, Q.; Wang, Y.; Zhang, J. UniProt: The Universal Protein Knowledgebase in 2023. *Nucleic Acids Res.* **2023**, *51*, D523−D531.

(29) McCoy, A. J.; Grosse-Kunstleve, R. W.; Storoni, L. C.; Read, R. J. Likelihood-Enhanced Fast Translation Functions. *Acta Crystallogr., Sect. D: Biol. Crystallogr.* **2005**, *61*, 458−464.

(30) Winn, M. D.; Ballard, C. C.; Cowtan, K. D.; Dodson, E. J.; Emsley, P.; Evans, P. R.; Keegan, R. M.; Krissinel, E. B.; Leslie, A. G. W.; McCoy, A.; McNicholas, S. J.; Murshudov, G. N.; Pannu, N. S.; Potterton, E. A.; Powell, H. R.; Read, R. J.; Vagin, A.; Wilson, K. S. Overview of the CCP4 Suite and Current Developments. *Acta Crystallogr., Sect. D: Biol. Crystallogr.* **2011**, *67*, 235−242.

(31) Murshudov, G. N.; Vagin, A. A.; Dodson, E. J. Refinement of Macromolecular Structures by the Maximum-Likelihood Method. *Acta Crystallogr., Sect. D: Biol. Crystallogr.* **1997**, *53*, 240−255.

(32) Emsley, P.; Cowtan, K. Coot: Model-Building Tools for Molecular Graphics. *Acta Crystallogr., Sect. D: Biol. Crystallogr.* **2004**, *60*, 2126−2132.

(33) Long, F.; Nicholls, R. A.; Emsley, P.; Gražulis, S.; Merkys, A.; Vaitkus, A.; Murshudov, G. N. AceDRG: A Stereochemical Description Generator for Ligands. *Acta Crystallogr., Sect. D: Struct. Biol.* **2017**, *73*, 112−122.

(34) Pettersen, E. F.; Goddard, T. D.; Huang, C. C.; Meng, E. C.; Couch, G. S.; Croll, T. I.; Morris, J. H.; Ferrin, T. E. UCSF ChimeraX: Structure Visualization for Researchers, Educators, and Developers. *Protein Sci.* **2021**, *30*, 70−82.

https://doi.org/10.1021/acs.jmedchem.3c00710
J. Med. Chem. XXXX, XXX, XXX−XXX